Gas-solid carbonation as a possible source of carbonates in cold planetary environments

Alexandre Garenne, German Montes-Hernandez, Pierre Beck, Bernard Schmitt, Olivier Brissaud, Antoine Pommerol

Gas-solid carbonation as a possible source of carbonates in cold planetary environments

A. Garenne[a,*], G. Montes-Hernandez[a,*], P. Beck[b], B. Schmitt[b], O. Brissaud[b], A. Pommerol[c]

[a] CNRS and University Joseph Fourier, ISTerre/UMR 5275, OSUG/INSU, BP 53, 38041 Grenoble Cedex 9, France

[b] CNRS and University Joseph Fourier, IPAG, OSUG/INSU, BP 53, 38041 Grenoble Cedex 9, France

[c] Physikalisches Institut, Universität Bern, Sidlerstrasse 5, CH-3012 Bern, Switzerland

*Corresponding authors: A. Garenne and G. Montes-Hernandez

Tel: Alexandre.Garenne: +33 (0)607912561

German. Montes-Hernandez : +33 (0)683363044

E-mail addresses: alexandre.garenne@obs.ujf-grenoble.fr and german.montes-hernandez@obs.ujf-grenoble.fr

Abstract

Carbonates are abundant sedimentary minerals at the surface and sub-surface of the Earth and they have been proposed as tracers of liquid water in extraterrestrial environments. Their formation mechanism is since generally associated with aqueous alteration processes. Recently, carbonate minerals have been discovered on Mars' surface by different orbital or rover missions. In particular, the phoenix mission has measured from 1 to 5% of calcium carbonate (calcite type) within the soil (Smith P.H. et al., 2009). These occurrences have been reported in area were the relative humidity is significantly high (Boynton et al., 2009). The small concentration of carbonates suggests an alternative process on mineral grain surfaces (as suggested by Shaheen et al., 2010) than carbonation in aqueous conditions. Such an observation could rather point toward a possible formation mechanism by dust-gas reaction under current Martian conditions. To understand the mechanism of carbonate formation under conditions relevant to current Martian atmosphere and surface, we designed an experimental setup consisting of an infrared microscope coupled to a cryogenic reaction cell (IR-CryoCell setup). Three different mineral precursors of carbonates (Ca and Mg hydroxides, and a hydrated Ca silicate formed from Ca_2SiO_4), low temperature (from -10 to +30°C), and reduced CO_2 pressure (from 100 to 2000 mbar) were utilized to investigate the mechanism of gas-solid carbonation at mineral surfaces. These mineral materials are crucial precursors to form Ca and Mg carbonates in humid environments (0 < relative humidity < 100%) at dust-CO_2 or dust-water ice-CO_2 interfaces. Our results reveal a significant and fast carbonation process for Ca hydroxide and hydrated Ca silicate. Conversely, only a moderate carbonation is observed for the Mg hydroxide. These results suggest that gas-solid carbonation process or carbonate formation at the dust-water ice-CO_2 interfaces could be a

currently active Mars' surface process. To the best of our knowledge, we report for the first time that calcium carbonate can be formed at a negative temperature (-10°C) via gas-solid carbonation of Ca hydroxide. We note that the carbonation process at low temperature (<0°C) described in the present study could also have important implications on the dust-water ice-CO2 interactions in cold terrestrial environments (e.g. Antarctic).

Keywords: Carbonates; Gas-solid carbonation; Mars; Low temperature; Infrared Microscopy; Ca and Mg Hydroxides.

66 **1. Introduction**

67 The biotic and abiotic (i.e. chemical) formation of carbonates plays a crucial role in the
68 global carbon cycle on Earth. In addition, carbonate minerals often sequester various trace
69 elements (actinides and lanthanides), metalloids, and heavy metals, and thus control in part their
70 global cycling (e.g. Paquette and Reeder, 1995; Stumm and Morgan, 1995; Sigg et al., 2000). In
71 general, carbonate minerals can be formed in natural or artificial environments by three different
72 mechanisms (e.g. Montes-Hernandez et al., 2010a): (1) aqueous nucleation-growth in
73 homogeneous or heterogeneous systems (aqueous conditions), for example, the chemical or
74 biogenic formation of carbonates in lakes, oceans, CO_2 storage sites, natural caves; (2) gas-solid
75 carbonation of alkaline minerals (fine particles) in the presence of adsorbed water (water
76 humidity conditions, $0 <$ water activity < 1), for example carbonate formation in water-
77 unsaturated soils, in terrestrial or extraterrestrial aerosols (Shaheen et al., 2010). This water has
78 an important role in the surface chemistry of minerals as was shown by Galhotra et al., (2009)
79 and Baltrusaitis and Grassian (2005) with zeolites and iron oxide surfaces; (3) dry gas-solid
80 carbonation of granular/porous materials (dry conditions, water activity ≈ 0), for example, the
81 industrial mineralization, recovery or capture of CO_2 at high temperatures in presence of alkaline
82 binary oxides (CaO, MgO) or metastable, nanoparticle alkaline silicates (Montes-Hernandez et
83 al., 2012).

84 In the Planetary Sciences context, carbonates are generally considered as indicators of
85 aqueous alteration processes (Bandfield et al., 2003; Milliken and Rivkin, 2009; Boynton et al.,
86 2009; Ehlmann et al., 2008; Michalski and Niles, 2010). In the case of Mars, huge deposits of
87 surface carbonates remained undetected for a long period, and their suspected absence was used

88 to constrain the chemistry of a putative Martian ocean (Fairén et al., 2004). Evidences are now
89 growing for the presence of carbonates at the surface of the red planet, which include
90 observations of carbonate-rich outcrops (Ehlmann et al., 2008; Michalski and Niles, 2010) as
91 well as carbonates within the Martian dust (Bandfield et al., 2003; Boynton et al., 2009). The
92 aqueous alteration of mafic rocks in the presence of CO_2 is certainly an efficient mechanism for
93 carbonate synthesis, an alternative pathway of carbonate synthesis exists, which does not require
94 the presence of liquid water. This pathway involves reaction of a mineral substrate with CO_2 in
95 the presence of chemisorbed water (few angstroms to few nm thick layers), and was recently
96 tested and observed for terrestrial aerosols (Shaheen et al., 2010).

97 Here, we report on an experimental study of the kinetic of carbonation in liquid-water free
98 environment. We designed novel, state of the art experimental setup (IR-CryoCell) to investigate
99 the *in-situ* gas-solid carbonation (i.e. resolved in time), for temperature and pressure conditions
100 relevant to Mars. We studied carbonate synthesis starting from Ca and Mg hydroxides and an
101 amorphous silicate (synthesized from Ca_2SiO_4), at low temperature (from -10 to +30°C) and at
102 low CO_2 pressure (from 100 to 2000 mbar). These starting materials are known precursors to
103 form respective Ca and Mg carbonates in humid environments at dust-CO_2 or dust-water ice-CO_2
104 interfaces, at least under « terrestrial » conditions. They also can be expected to occur at the
105 surface of Mars and some asteroids (Mg hydroxide has been described on Ceres). We report here
106 laboratory experiments on gas-solid carbonation process at low temperature (<0°C), which
107 provides new insights on conditions for carbonate formation. We will show that gas-solid
108 carbonation can occur below the water frost point (at terrestrial atmospheric pressure), with
109 significant implications on the dust/water-ice/CO_2 interactions in cold environments.

2. Materials and methods

The experiments were performed using three different materials, Ca, Mg hydroxide and a Ca silicate hydrate. CO_2 is known to react with surface of CaO and MgO by adsorption (Ochs et al., 1998a; Ochs et al., 1998b) and produce carbonates as well the importance of OH groups to water adsorption on surfaces (Yamamoto et al., 2008). These substrates were chosen to mimic natural conditions and to catalyze reaction as their surfaces are terminated by OH groups: i) in order to form Ca-Mg carbonate by reaction with CO_2, a Ca and Mg source is needed; ii) the presence of hydroxyl groups in the starting material was requested to permit auto-catalysis of the reaction (Montes-Hernandez et al., 2010a); iii) the material had to be geologically relevant.

Brucite has not been detected on the Martian surface. However, various types of phyllosilicates have been now described over the planet, that are interpreted as aqueous alteration products of mafic rocks (see the recent review by Ehlmann et al., 2011). Such aqueous alteration processes can be accompanied by the production of brucite (Evans, 2008). Identification of brucite by its spectral properties is difficult since no diagnostic band is present in the NIR, with the exception of the 2.7 micrometer feature ubiquitous to almost all -OH bearing phases. Brucite has been diagnosed on some asteroids from observations in the mid-IR (together with carbonate). It is the case of the largest main-belt object, Ceres. In addition, MgO has been proposed as a condensation product in some solar nebula models, which should readily transform to brucite in the presence of gaseous water or humidity (Gail and Sedlmayr, 1999).

Portlandite has not been reported on Mars either. On Earth, it is almost always found in association with calcium carbonates, and is very difficult to observe due to its high reactivity with CO_2. We chose to study portlandite because of its high catalytic reactivity which enabled to

provide kinetic measurements under some hours. In addition, it is a structural analog to brucite and a number of X-$(OH)_2$ type hydroxide compounds (where X=Ni, Co, Fe, Mn, Cd). CaO has also been proposed as an intermediate compound by Shaheen et al. (2010) to explain the formation of calcium carbonate on Mars, which could readily transform to portlandite in the presence of gaseous H_2O or humidity.

Finally, we used an amorphous calcium silicate hydrate synthesized from larnite (Ca_2SiO_4). This material was chosen to represent an amorphous volcanic material. Volcanic activity has been widespread on Mars, and volcanoclastic deposits have been described (Ehlmann et al., 2011). We decided to use a pure calcium amorphous silicate (rather than a basaltic glass), in order to simplify the chemistry of the system. However, one might expect a more complex chemistry for Martian volcanic glasses. Our approach might appear too simplistic, but might provide grounds for understanding more complex chemistries.

2.1. Materials

Portlandite: Calcium hydroxide $Ca(OH)_2$ was provided by Sigma-Aldrich with 96% chemical purity (about 3% of $CaCO_3$) and 1% of other impurities. This material is characterized by platy nanoparticles (sheet forms) forming micrometric aggregates with high porosity and/or high specific surface area (15 m^2/g). Its infrared spectrum has revealed a small amount of adsorbed water at atmospheric conditions, around $0{,}01 g H_2O/g Ca(OH)_2$ determinated by TGA. The portlandite sample was used without any physicochemical treatment.

Brucite: Magnesium hydroxide $Mg(OH)_2$ was provided by Fisher Scientific (UK). This material

153 is characterized by platy hexagonal microparticles. A small amount of adsorbed water at
154 atmospheric conditions was detected by infrared spectroscopy. The brucite sample was crushed in
155 a mortar before use.

156 **Amorphous calcium silicate hydrate:** This material was synthesized from synthetic larnite
157 mineral (Ca_2SiO_4) by using a simple acidic treatment (2M HCl solution) at room lab temperature
158 during 15 minutes. Then, consecutive dilutions with demineralized water were carried out until
159 pH equal to 3. Finally, the solid was separated from the solution by centrifugation (10 minutes at
160 12000 rpm) and dried directly in the centrifugation flasks at 80°C for 48h. The larnite synthetic
161 mineral was provided by A. Santos and it was synthesized as reported in Santos et al. (2009).

162 **Carbon dioxide:** Carbon dioxide CO_2 was provided by Linde Gas S.A. with 99.995% of
163 chemical purity. This gas was directly injected in the cryogenic reaction cell without any
164 treatment or purification.

165 *2.2. Infrared microscope*

166 An infrared microscope (BRUKER HYPERION 3000) coupled with a cryogenic cell (designed
167 and built at IPAG) was used to obtain infrared spectra in transmission mode. The IR beam was
168 focused trough a 15x objective and the typical size of the spot on the sample was around 50x50
169 μm^2. The spectral resolution was $4cm^{-1}$ and the spectra were recorded in transmission mode
170 between $4000cm^{-1}$ and $700cm^{-1}$.

171 *2.3. Cryogenic cell*

172 An environmental cell was designed and built at IPAG in order to simulate low CO_2 pressure and

low temperature (LP-LT) close to Martian atmospheric conditions. A heating resistance coupled to a liquid N_2 circuit (77K) allows an efficient regulation of sample temperature from -180°C to +100°C. Additionally, a turbomolecular vacuum pump and a CO_2 cylinder were connected to reach a secondary vacuum and to inject a controlled CO_2 pressure into the reaction cell, respectively. Figure 1 shows a schematic diagram of all main parts of the IR-CryoCell setup.

2.4. Gas-solid carbonation experiments

For these measurements, the reacting $Ca(OH)_2$ particles, stored at atmospheric conditions, were manually deposited and compressed as a thin film on a KBr window. Then the KBr window was carefully placed in the reaction cell to be assembled to the microscope. All carbonation experiments have been carried out in presence of molecular water (adsorbed or crystallized as ice depending on the carbonation temperature) which catalyze the carbonation process. The carbonation temperatures used in this study were -10, 0, 10, 25 or 30°C and the CO_2 pressures were typically 100, 1000 and 2000 mbar. This pressure is higher than Martian pressure to accelerate the reaction due to a daily timescale limitation by the experimental setup. We note that the CO_2 gas has been directly injected into the reaction cell in presence or absence of atmospheric air. For the latter case, we started by fixing the water adsorbed onto the solid by cooling the cell at -60°C before making a high vacuum pumping for 10 min in order to remove exclusively the air from the reaction cell. After injection of CO_2 10 to 15 infrared spectra have been collected as a function of time until an apparent spectroscopic equilibrium state is reached (3-6h). Complementary carbonation experiments have been carried out by using Mg hydroxide (brucite: $Mg(OH)_2$) and the amorphous calcium silicate hydrate as solid reactants, but, for these cases the carbonation temperature has been fixed at 25°C and 1 bar of CO_2 has been injected into the

195 reaction cell without air removal (more reacting system).

196 Each carbonation experiment has been repeated 2 times in order to verify its reproducibility. All
197 carbonation experiments and their physicochemical conditions are summarized in Table 1.

198 *2.5. Calculation of integrated band intensities*

199 The gas-solid carbonation of calcium hydroxide at low temperature (<30°C) in presence of
200 adsorbed water can be expressed by a global reaction as follows:

201 $Ca(OH)_2(s) + CO_2(g) => CaCO_3(s) + H_2O(v\text{-}l)$ (1)

202 Generally, this global reaction is incomplete due to the formation of a protective carbonate layer
203 around the reacting particle which restricts or stops the CO_2 transfer at the grain or aggregate
204 scale (Montes-Hernandez et al., 2010a). In the present study, the integrated band intensities for
205 hydroxyl (-OH), carbonate (CO_3^{2-}) and H_2O functional groups, concerning reaction (1) at an
206 instant *t* have been estimated by using a Trapezoidal rule integration. A wavenumber interval and
207 a characteristic continuum have been manually defined to determine the intensity of a given band
208 depending on the initial reactant. For example, in the gas-solid carbonation experiments with
209 $Ca(OH)_2$ particles, two continuums have been defined as linear segments over two different
210 spectral ranges, one for the -OH at 3640 cm^{-1} and H_2O at 3450 cm^{-1} band intensities and the other
211 for the H_2O at 1650 cm^{-1} and CO_3^{2-} at 1420 cm^{-1} band intensities (see Figure 2).

212

213 *2.6. Fitting of the kinetic experimental-calculated data for gas-solid carbonation*

214 Several kinetic models (first-order, pseudo-first-oder, second-order, pseudo-second-order,
215 reversible one, irreversible one...) are generally used for fitting kinetic experimental data of
216 sorption and adsorption systems (Ho and McKay, 1999; Ho, 2006). For our experiments, we

have chosen pseudo-second-order model because it was successfully applied in previous studies (Montes-Hernandez and Geraud, 2004 ; Montes-Hernandez and Rihs, 2006; Montes-Hernandez et al., 2009, 2010a, 2010b, 2012a, 2012b) and can be adequately used to fit experimental data of carbonation process as demonstrated in Montes-Hernandez et al., 2009. This model reproduces a process consisting of a fast mass transfer followed by a second step of slower mass transfer until equilibrium is achieved. It can be written in its differential form as follows:

$$\frac{dA^{CO3},_t}{dt} = Kc\left(A^{CO3},_{max} - A^{CO3},_t\right)^2 \quad (2)$$

Where $A^{CO3},_t$ is the integrated band intensity for the carbonate group at a given time, *t* [minutes], corresponding to carbonation extent; $A^{CO3},_{max}$ is the maximum extend of carbonation at equilibrium; Kc is the rate constant of $Ca(OH)_2$ carbonation.

The second step (until equilibrium) is interpreted by as a passivation effect due to the formation of a protective carbonate layer (Montes-Hernandez et al., 2012a). In this study, the increase of integrated band intensity with time for the carbonate group (CO_3^{2-}), i.e. during gas-solid carbonation process, has been fitted by using a kinetic double-pseudo-second-order model. This model assumes two kinetic regimes due to the presence of two types of reactive surface sites. The integrated form of the double kinetic model is given by the following hyperbolic equation:

$$A^{CO3},_t = \frac{\left(A^{CO3},_{max1}\right)t}{\left(t_{1/2_1} + t\right)} + \frac{\left(A^{CO3},_{max2}\right)t}{\left(t_{1/2_2} + t\right)} \quad (3)$$

Where $A^{CO3},_t$ is the integrated band intensity for the carbonate group at a given time, *t* [minutes],

corresponding to carbonation extent; $A^{CO3}_{,max1}$ and $A^{CO3}_{,max2}$ are the maximum extent of carbonation at apparent equilibrium for both kinetic carbonation regimes, respectively; $t_{1/2_1}$ and $t_{1/2_2}$ are the half-carbonation times for both kinetic carbonation regimes, respectively. In other terms, the half-carbonation times represent the times after which half of the maximum of kinetic carbonation regimes (expressed as maximum of integrated band intensities for carbonate group) is obtained. The fitting of kinetics data allow an estimation of these parameters and was performed by a non linear regression by least-squares method. These simple parameters are used in this study to evaluate the kinetic effects of temperature, CO_2 pressure and nature of the solid on the gas-solid carbonation process.

The activation energy (Ea, Table 1) of the reaction was calculated assuming an Arrhenius behavior for the initial carbonation rate. We have used 4 points to calculate Ea for carbonation experiments of portlandite (at the temperature of -10°C,0°C,10°C and 30°C, for both experiments performed under 1 bar and 2 bar CO_2).

3. Results

3.1. Gas-solid carbonation of $Ca(OH)_2$ particles at low temperature (<0°C)

Very few experimental studies have characterized the carbonate formation or CO_2 mineralization at the mineral-ice water-CO_2 interfaces on Earth and planetary cold-environments (e.g. Antarctic and Mars surface). In our study, several gas-solid reactions carried out in the cryogenic cell coupled to the infrared microscope reveal that carbonate formation or CO_2 mineralization is possible at low temperature (-10°C and 0°C) using a simplified analogue $Ca(OH)_2$(mineral)-

257 water(adsorbed)-CO_2(gas) system (see Fig. 3 (c) to (f)). The results displayed in Figure 3 also
258 reveal that the carbonation extent, monitored *in-situ* by an increase of carbonate band intensity at
259 1420 cm^{-1}, is clearly inhibited by a decrease of temperature from 30°C to -10 °C. The increase of
260 integrated band intensity with time for the carbonate group at 1420 cm^{-1} has been successfully
261 fitted by using the kinetic double-pseudo-second-order model. The experimental data and the
262 calculated fits for six experiments are plotted in Figure 4. This "a posteriori" modeling shows the
263 good fits of all the experimental data by such type of kinetic model (correlation coefficient, R
264 close to 1), and confirms the inhibition effect of temperature and the effect of relative humidity
265 on the carbonation extent and kinetic parameters (see also Table 1).

266 One additional carbonation experiment with $Ca(OH)_2$ particles was carried out at low CO_2
267 pressure (100 mbar) and at moderate temperature (25°C). For this case, the initial air contained
268 into the cell was previously removed by pumping to secondary vacuum at low temperature (-
269 60°C) as explained in the materials and methods section. Here, a significant carbonation is
270 observed after 4 minutes of $Ca(OH)_2$-CO_2 interaction followed by a very slow carbonation step
271 until an apparent spectroscopic equilibrium is possibly reached (about 6h) (see Fig. 5). These
272 experimental data have been also successfully fitted by using the kinetic double-pseudo-second-
273 order model. A last carbonation experiment was performed at a CO_2 pressure of 2 bar (at 25 °C)
274 in order to compare with the low CO_2 pressure experiments. A significant carbonation was
275 observed during all the experiment (see Fig. 6), which was fitted with the kinetic-pseudo-second
276 order model.

277 *3.2. Gas-solid carbonation of Mg hydroxide*

278 The gas-solid carbonation depends also on the nature of the solid. For this reason one other

279 powdered material, Mg hydroxide (synthetic brucite), was investigated specifically at higher
280 reactive conditions (25°C and 1bar of CO_2, in presence of air). To form Mg carbonates, the most
281 simple materials as starting reactant are binary oxides or hydroxides in the precursor material.
282 Brucite particles are found to be only slightly carbonated at these T-P_{CO2} conditions after 5.5h of
283 $Mg(OH)_2$-CO_2 interaction (see Figure 7). These *in-situ* infrared measurements clearly reveal that
284 the Mg hydroxide (brucite) is more chemically stable than Ca hydroxide (portlandite) under a
285 CO_2-rich atmosphere at a given relative humidity. In summary, the gas-solid carbonation of Ca
286 and Mg hydroxides depends on the experimental conditions employed (i.e. T, P_{CO2}, relative
287 humidity) and on the intrinsic properties of solid (i.e. hydrophilicity, particle size, specific surface
288 area, and chemical stability).
289 Finally, a kinetic regime and the maximum carbonation extent at an apparent equilibrium
290 ($A^{CO3}_{,max1} + A^{CO3}_{,max2}$) is successfully determined by using a kinetic double-pseudo-second-order
291 model (see Fig. 7 (c)).
292 *3.3. Gas-solid carbonation of an amorphous calcium silicate hydrate*
293 A last materials, an amorphous calcium silicate hydrate, has been investigated at higher reactive
294 conditions (25°C and 1bar of CO_2, in presence of air) to test the gas-solid carbonation efficiency.
295 The amorphous calcium silicate hydrate, is significantly carbonated via gas-solid carbonation at
296 the above mentioned T-P_{CO2} conditions after 8h of reaction (see Figure 8), which suggests
297 chemical stability has a significant impact on the efficiency of the carbonation.
298 Finally, a kinetic regime and the maximum carbonation extent at apparent equilibrium ($A^{CO3}_{,max1}$
299 + $A^{CO3}_{,max2}$) is also successfully determined by using the kinetic double-pseudo-second-order
300 model (see Fig. 8 (c)).
301

4. The mechanism of carbonation

All the experiments with the Ca and Mg hydroxides show an increase of the band intensities of carbonates, at low temperature and low pressure. In this study we assume that part of the water initially adsorbed onto $Ca(OH)_2$ particles was partially crystallized by cooling when the temperature is negative (<0°C). The presence of an ice layer limits the access of CO_2 molecules to nanopores, and therefore limiting the CO_2 access to the local CO_3^{2-} production ($CO_2(g)+H_2O(adsorbed)=>CO_3^{2-}+2H^+$) required to form a carbonate layer around the $Ca(OH)_2$ particles (see also: Montes-Hernandez et al. 2010a). Strictly speaking, the relative humidity is not controlled in our experiments; however, two experiment protocols implying atmospheric vapor have been designed, firstly, direct injection of CO_2 gas into the reaction cell initially filled with air, i.e. at lab relative humidity (CO_2-air system) and secondly, the injection of CO_2 gas after removal of the air by secondary vacuum pumping at low temperature (-60°C) (CO_2 system). The difference between these experiments could explain why the carbonation extent decreases when the initial air (contained into the reaction cell) is removed (see comparisons (c) and (d) or (e) and (f) in Fig. 3). We can assume a similar relative humidity of the lab room for all experiments. The relative humidity has clearly an impact on the carbonation efficiency, the experiments without air (very low relative humidity) showing a lower amount of carbonation at low temperature.

The fit of the data by the kinetic model assumes two kinetic regimes, usually due to the presence of two types of reactive surface sites. In our carbonation experiments, the formation of a hydrated carbonate layer around the core of reacting $Ca(OH)_2$ particles produces a complex passivation step, possibly perturbed by three simultaneous physicochemical processes: (1) solid state transformation from hydrated calcium carbonate to calcite and/or from aragonite to calcite, (2) partial expelling of produced molecular water during the carbonation process (see Eq. (1)) and (3)

local acidification by an excess of molecular water in pores or onto surfaces (H_2O(produced)+ CO_2(g) =>HCO_3^- + H^+). In summary, the complex kinetic behavior related to gas-solid carbonation of $Ca(OH)_2$ particles is successfully described applying two kinetic regimes. A schematic representation of this carbonation process is illustrated in Figure 9. The rate of carbonation depends on the access to the nanopores of the material by the CO_2. These pores have to be water-unsaturated to facilitate access of the CO_2 gas to react with the minerals. The pressure has a strong impact on the rate and yield of carbonation. In the case of the low pressure experiments, a two stage kinetic model was shown to fit the data. Experiments revealed a fast carbonation during a short time (stage 1) followed by a slower carbonation (stage 2). The magnitude of carbonate formation is high in stage 1 and lower in stage 2. In the case of the experiments performed at higher CO_2 pressure (2 bar) (fig. 6.c) a two stage reaction is also observed. However, unlike the low pressure experiments, the magnitude of carbonation achieved in stage 2 is quite significant.

For the low pressure experiments, we suspect that the intraparticle diffusion of CO_2, possibly limited by the low gas pressure in the system (100 mbar of CO_2), is the rate limiting step due to the carbonate layer which strongly reduce the diffusion of the gas. This rate limiting step is no more observed at high CO_2 pressure (>20 bar). In this case, the $Ca(OH)_2$ particles are completely carbonated, leading to the formation of calcite nano-crystals (Montes-Hernandez et al., 2010b). We can assume a correlation between the pressure and the thickness of the layer that transforms to carbonate by gas-solid reaction. The effect of CO2 pressure observed in explained by the presence of passivation step and the formation of carbonate layer through which CO2 molecules have to diffuse. Therefore in the case of an uncarbonated material, the effect of CO_2 pressure on the initial reaction rate is expected to be moderate. Although the CO_2 pressure on Mars (about 10

mbar) is lower than CO_2 pressures used in our experiments (100 mbar), it is likely that our results can be extrapolated to Martian atmospheric CO_2 pressure.

Unfortunately, the gas-solid carbonation mechanism of amorphous calcium silicate hydrate is not elucidated due to its unknown atomic organization. However, we assume that the abundant molecular water adsorbed onto the solid plays a crucial role to start the gas-solid carbonation process at the investigated conditions. The *in-situ* infrared measurements reveal two important insights: (1) The expelling of pre-existent molecular water in/on the solid towards the gas phase during the carbonation process. This is attested by a clear decrease of the stretching and bending band intensities of water (see Fig. 8 (a) and (b)), (2) Similar to carbonation of Ca hydroxide, the formation of calcite and aragonite are mainly identified, the formation of hydrated calcium carbonate being only suspected (see also Montes-Hernandez et al. 2010a)

5. Discussion

Carbonates have been found on Mars in two kinds of geological settings: (i) outcrops of carbonates, identified in the Nili Fossae region (Ehlmann et al., 2008), in the central peak of Leighton crater (Michalski and Niles, 2010) and in the Columbia Hills of Gusev crater (Morris et al., 2010); and (ii) carbonates-bearing dust, identified by the TES instrument (Bandfield et al., 2003) and the phoenix lander (Boynton et al., 2009). In the case of the outcrops from the Columbia Hills and Nili Fossae, carbonates are present as major components (16 to 34 wt % in the case of the Columbia Hills, about 80 % in the case of Nili Fossae), and their derived

chemistry is similar to that of carbonates found in Martian meteorites (Mittlefehldt, 1994), i.e. Fe-Mg carbonates. The association of these carbonate outcrops with phyllosilicates advocate for a possible hydrothermal origin of these carbonates, a phenomenon that has been reproduced in laboratory experiments (Golden et al., 2000) and that is observed in some terrestrial hydrothermal systems (Treiman et al., 2002; Brown et al., 2010). However, it is well known that terrestrial alteration of mafic rocks can produce brucite as a primary alteration product (Xiong and Snider Lord, 2008), which should readily transform into carbonate by interaction with the Martian atmosphere, according to our experiments. The observed carbonates outcrops could rather be former outcrops of brucite-rich sedimentary rocks, that were subsequently altered to carbonates by interaction with the atmosphere.

In the case of carbonates observed in the Martian dust, both magnesite (Bandfield et al., 2003) and calcite (Boynton et al., 2009) have been reported, and their typical abundance is below 5 %. Although aqueous formation has received widespread attention for this type of occurrence of carbonates on Mars, we propose gas-solid reaction as a possible formation mechanism. Calcite formation at the dust-CO_2 interfaces requires a source of calcium (e.g. Ca binary oxides or an amorphous metastable Ca silicate) possibly coming from volcanic activity (Shaheen et al., 2010), mechanical erosion or extra-Martian particulate matter (including meteorite impacts, interstellar dusts). A large diversity of phyllosilicates and hydrated phyllosilicates was found on the Martian surface (Mustard et al., 2008; Jänchen et al., 2006; Fairén et al., 2009; Murchie et al., 2009; Ehlmann et al., 2011). As we have shown, the presence of molecular water is also required because hydration of the Ca precursor is assumed to be a crucial step prior to the carbonation process. Laboratory studies of Martian analogs suggest that adsorbed water should be present in significant amount within the Martian soil (Pommerol et al., 2009; Beck et al., 2010; Jänchen et

394 al., 2006) and adsorbed water has been also detected by infrared spectroscopy (Poulet et al.,
395 2009). In addition, the gamma rays and neutrons spectrometers on Mars Odyssey have shown
396 evidence for the presence of water in the first meter of the martian subsurface (Feldman et al.,
397 2004). A simplified scenario for calcite formation at the dust-CO_2 interfaces and its natural
398 deposition on the soil is schematically illustrated in Fig. 10. In this scenario we assume that the
399 precursor, a calcium hydroxide with adsorbed water, is produced by atmospheric alteration of
400 volcanic CaO particles in the atmosphere. Reactant minerals such as portlandite could be difficult
401 to detect on Mars by reflectance spectroscopy due to the carbonate layer around the calcium
402 hydroxide. In the case of hydromagnesite, the presence of brucite is required somewhere on
403 Mars, which would be subsequently transformed to carbonates, eroded, and transported. As we
404 stated earlier, brucite should form in association with phyllosilicates during the aqueous alteration
405 of mafic rocks.

406 The efficiency of carbonates synthesis on Mars by gas-solid reaction will depend on the
407 mineral substrate (as we showed, brucite, portlandite and larnite have distinct synthesis kinetics),
408 the local temperature, the atmospheric humidity, and likely the atmospheric pressure (which can
409 substantially vary with season as well as with topography). Even at temperatures below the frost
410 point, carbonates synthesis can occur by gas-solid reaction, on a daily timescale (table 1). On
411 Mars, the water vapor pressure is low (P_{H2O} about 10 Pa) and the frost point is depressed with
412 regard to that on Earth. Given the present knowledge of the water vapor surface pressure, a
413 typical value of 200 K is found for the frost point on the Martian surface (Schorghofer and
414 Aharonson., 2005). Such temperature typically corresponds to seasonal average around 60° in
415 latitude.

416 The relative humidity on Mars fluctuates on a daily basis. At the Phoenix landing site (Smith P.H.

et al., 2009) it is measured around 5% during Martian day time, close to saturation early night and saturating at the end of the night. Carbonate synthesis will be accelerated by a high atmospheric humidity, which can occur during the warmer season. TES instrument on Mars Global Surveyor has water vapor evolution during 2 martian years, and the maximum was found during midsummer in the northern hemisphere with 100 pr-µm (Smith M.D., 2002,2004). The maximum water vapor measured by Mars Express instruments (OMEGA and SPICAM) is found during midsummer, around 60 pr-µm content. This maximum is observed at latitude 75-80°N and longitudes 210-240°E (Fouchet et al., 2007; Fedorova et al., 2006; Melchiorri et al.,2007)), an area is close to Phoenix landing site (latitude 68°N and longitude 233°E).

Current Global Circulation Models (GCM) of Mars can be used to determine the optimal locations and times for the gas-solid synthesis of carbonates. Simulations with Mars Climate Database (Forget et al., 1999, 2006) estimated high relative humidity (around 70%) and temperatures close to -20°C during mid summer (L_s =120°) in the Phoenix landing site area (at 12 a.m). These conditions are sufficient to initiate the carbonation reaction according to our experiments, and carbonates were observed in the Phoenix soil (Smith et al., 2009)

Mars is not the only extra-terrestrial body where carbonates have been detected, this is also the case of Ceres, the largest asteroid in the main belt. Its shape is close to hydrostatic equilibrium and its bulk density suggests the presence of ice in its interior (Thomas et al., 2005). The surface of Ceres shows a well-resolved 3-µm absorption band, which interpretation has been debated (Lebofsky et al., 1981; Vernazza et al., 2005; Rivkin et al., 2006; Rivkin et al., 2011; Beck et al., 2011). In a recent study, Milliken and Rivkin (2009) combined NIR and MIR observations of Ceres' surface and successfully modeled both spectral regions with a combination

440 of brucite, carbonate and a Fe-rich phyllosilicate. Such a mineralogical assemblage was explained
441 by aqueous alteration of mafic silicates in the presence of CO_2, by analogy with the processes
442 inferred from the mineralogy of hydrated meteorites that can present a significant amount of
443 carbonates (Zolensky et al., 2002). If brucite is rare in the mineralogy of hydrated chondrites, it is
444 a common product of aqueous alteration of terrestrial rocks. The condition of brucite formation is
445 specific in terms of T, pH and pO_2, and source rock. If the formation of carbonate by reaction of
446 brucite with water is possible, gas-solid reaction cannot be excluded. This mechanism could
447 occur at some depth in the asteroid body, where CO_2 pressure can build-up. However, because of
448 the low temperature at the surface of Ceres, long timescales are expected for such a process.
449 Further consideration would require an accurate knowledge of the kinetics of the gas-solid
450 carbonation.
451
452 Finally, the carbonate synthesis mechanism that we described is certainly active on Earth,
453 where carbonate minerals played an important role in the planet evolution. Many studies are
454 available about carbonate reactivity and synthesis in liquid-water but information on its behavior
455 at sub-zero temperatures (for example solubility in frozen water) are sparse. The results we
456 obtained reveal that gas-solid carbonation can occur at sub-zero temperature, in the presence of
457 gaseous CO_2 and H_2O. These conditions are present on Earth in arctic regions and in the upper
458 atmosphere. This mechanism can thus occur on the availability of the adequate precursor.
459 The presence of oxygen isotope anomalies in carbonates from terrestrial aerosols
460 (Shaheen et al., 2010) suggests a carbonation by exchange with ozone. Such a result suggests a
461 possible formation of carbonate by chemical reaction in the upper atmosphere, from a CaO
462 precursor. We can propose hydration of $CaO_{(s)}$by $H_2O_{(g)}$, and successive reaction of $Ca(OH)_{2(s)}$

463 with $CO_{2(g)}$ as a formation mechanism of these carbonates.

464 Calcium carbonate and carbonate hydrates have been found in arctic ice (Dieckmann et
465 al., 2008; Sala et al. 2008). The formation mechanism of these carbonates is a matter of active
466 research, since it could provide a major CO_2 sequestration process. Hydrous carbonates (for
467 instance ikaite) have been proposed to originate by precipitation during sea-ice formation, as
468 suggested by thermodynamical calculations. Anhydrous carbonates can have an origin as primary
469 aerosols, with a synthesis mechanism possibly similar to the one described in the previous
470 paragraph. In addition, in situ gas-solid formation is possible, depending on the availability of an
471 adequate precursor (as we showed here, an Ca or Mg hydroxides, or Ca-rich amorphous
472 silicates).

473

474 **6. Conclusion**

475 In this study, we designed an original experimental method to form carbonates via gas-solid
476 reaction in presence of adsorbed water. We used an infrared microscope coupled to a cryogenic
477 reaction cell (IR-CryoCell setup) to investigate this process with 3 different carbonate precursors
478 (Ca hydroxide (portlandite), Mg hydroxide (brucite), and an amorphous calcium silicate hydrate).
479 We demonstrated for the first time that calcium carbonate can be formed at low temperature
480 (<0°C) via gas solid carbonation of Ca hydroxide. Both amorphous Ca silicate hydrate and Ca
481 hydroxide were significantly carbonated at the investigated T-P_{CO2} conditions. Conversely, only a
482 very slight gas-solid carbonation of Mg hydroxide particles was detected by IR spectroscopy. We
483 extracted the kinetic parameters of the reaction from our measured carbonation curves, following
484 a kinetic double-pseudo-second-order model. From these results we can clearly state that the
485 conditions for gas-solid carbonation exist on Mars, and that this process could be the source of

the detected Ca and Mg carbonates found in the Martian dust and soil. These carbonates can be synthesized from a brucite precursor (a common hydrothermal product), from volcanic derived aerosols, as well as from extraterrestrial dust. This mechanism should be considered in future global modeling of the carbon cycle of the red planet, and might also be active in cold terrestrial deserts.

Acknowledgements

The authors are grateful to the French National Center for Scientific Research (CNRS), the French National Research Agency (ANR) and University Joseph Fourier (UJF) in Grenoble for providing the financial support.

References

Bandfield, J.L., Glotch, T.D. and Christensen, P.R. , 2003. Spectroscopic Identification of Carbonate Minerals in the Martian Dust. Science. 301, 1084-1087.

Beck, P., Pommerol, A., Schmitt, B. and Brissaud, O., 2010. Kinetics of water adsorption on minerals and the breathing of the Martian regolith. J.Geophys. Res.-Planets. 115, E10011

Beck, P., Quirico, E., Sevestre, D., Montes-Hernandez, G., Pommerol, A. and Schmitt, B. 2011. Goethite as an alternative origin of the 3.1mu m band on dark asteroids. Astron. Astrophys. 526, A85.

Baltrusaitis, J. and Grassian, V.H., 2005. Surface reactions of carbon dioxide at the adsorbed water-iron oxide interface. J Phys Chem B. 109, 12227–12230.

507 Boynton, W. V., Ming, D. W., Kounaves, S. P., Young, S. M. M., Arvidson, R. E., Hecht, M. H.,
508 Hoffman, J., Niles, P. B., Hamara, D. K., Quinn, R. C., Smith, P. H., Sutter, B., Catling, D. C.
509 and Morris, R. V., 2009 Evidence for Calcium Carbonate at the Mars Phoenix Landing
510 Site. Science. 325, 61-64.

511 Brown, A. J., Hook, S. J., Baldridge, A. M., Crowley, J. K., Bridges, N. T., Thomson, B. J.,
512 Marion, G. M., de Souza Filho, C. R. and Bishop, J. L., 2010. Hydrothermal formation of
513 Clay-Carbonate alteration assemblages in the Nil Fossae region of Mars. Earth Planet.
514 Sci. Lett. 297, 174-182.

515 Dieckmann, G.S., Nehrke, G., Papadimitriou, S., Göttlicher, J., Steininger, R., Kennedy, H.,
516 Wolf-Gladrow, D. and Thomas, D.N., 2008. Calcium carbonate as ikaite in Antartic sea
517 ice. Geophys. Res. Lett.35, L08501.

518 Ehlmann, B.L., Mustard, J.F., Murchie, S.L., Poulet, F., Bishop, J.L., Brown, A.J., Calvin, W.M.,
519 Clark, R.N., Des Marais, D.J., Milliken, R.E., Roach, L.H., Roush, T.L., Swayze, G.A.
520 and Wray, J.J., 2008. Orbital Identification of Carbonate-Bearing Rocks on Mars.
521 Science. 322, 1828-1832.

522 Ehlmann, B.L., Mustard, J.F., Murchie, S.L., Bibring, J.-P., Meunier, A., Fraeman, A.A. and
523 Langevin, Y., 2011. Subsurface water clay mineral formation during the early history of
524 Mars. Nature. 479, 53-60.

525 Evans, B.W., 2008. Control of the products of serpentinization by the Fe(2)Mg(1) exchange
526 potential of olivine and orthopyroxene. J. Petrol. 49, 1873-1887.

527 Fairén, A. G., Fernandez-Remolar, D., Dohm, J. M., Baker, V. R. and Amils, R., 2004. Inhibition

528 of carbonate synthesis in acidic oceans on early Mars. Nature. 431, 423-426.
529 Fairén, A.G., Davila, A.F., Gago-Duport, L., Amils, R. and McKay, C.P., 2009. Stability against
530 freezing of aqueous solutions on early Mars. Nature.459,401-404.
531 Fedorova, A., Korablev, O., Bertaux, J.-L., Rodin, A., Kiselev, A. and Perrier, S., 2006. Mars
532 water vapor abundance from SPICAM IR spectrometer: Seasonnal and geographic
533 distributions. J. Geophys. Res.111, E09S08.
534 Feldman, W.C., Prettyman, T.H., Maurice, S., Plaut, J.J., Bish, D.L., Vaniman, D.T., Mellon,
535 M.T., Metzger, A.E., Squyres, S.W., Karunatillake, S., Boynton, W.V., Elphic, R.C.,
536 Funsten, H.O. Lawrence, D.J. and Tokar, R.L., 2004. Global distribution of near-surface
537 hydrogen on Mars. J. Geophys. Res.109, E09006.
538 Forget, F., Hourdin, F., Fournier, R., Hourdin, C., Talagrand, O., Collins, M., Lewis, S. R., Read,
539 P. L., & Huot, J.-P. 1999. Improved general circulation models of the Martian atmosphere
540 from the surface to above 80 km. Journal of Geophysical Research, 1042, 24155–24176.
541 Forget, F., Millour, E., Lebonnois, S., Montabone, L., Dassas, K., Lewis, S. R., Read, P. L.,
542 López-Valverde, M. A., González-Galindo, F., Montmessin, F., Lefèvre, F., Desjean, M.-
543 C., & Huot, J.-P. 2006 (Feb.). The new Mars climate database. Page 128 of : F. Forget, M.
544 A. Lopez-Valverde, M. C. Desjean, J. P. Huot, F. Lefevre, S. Lebonnois, S. R. Lewis, E.
545 Millour, P. L. Read, & R. J. Wilson (ed), Mars Atmosphere Model ling and Observations.
546 Fouchet, T., Lellouch, E., Ignatiev, N.I., Forget, F., Titov, D.V., Tschimmel, M., Montmessin, F.,
547 Formisano, V., Guiranna, M., Maturilli, A. and Encrenaz, T., 2007. Martiann water vapor:
548 Mars Express PFS/LW observations. Icarus. 190, 32-49.
549 Gail, H.-P. and Sedlmayr, E., 1999. Mineral formation in stellar winds. Astron. Astrophys. 347,
550 594–616.

551 Galhotra, P., Navea, J.G., Larsen, S.C. And Grassian,V.H. , 2009. Carbon dioxide ((CO2)-O-16
552 and (CO2)-O-18) adsorption in zeolite Y materials: Effect of cation, adsorbed water and
553 particle size. Energ Environ Sci .2,401–409.
554 Golden, D. C., Ming, D. W., Schwandt, C. S., Morris, R. V., Yang, S. V. and Lofgren, G. E.,
555 2000. An experimental study on kinetically-driven precipitation of calcium-magnesium-
556 iron carbonates from solution: Implications for the low-temperature formation of
557 carbonates in martian meteorite Allan Hills 84001. Meteoritics Planet. Sci. 35, 457-465.
558 Ho, Y.S. and McKay, G., 1999. Pseudo-second order model for sorption processes. Process
559 Biochem. 34, 451-465
560 Ho, Y.S., 2006. Review of second order models for adsorption systems. J. Hazard Mater. B136,
561 681-689
562 Jänchen, J., Bish, D.L., Möhlmann, D.T.F. and Stach, H., 2006. Investigation of the water
563 sorption properties of Mars-relevant micro-and mesoporous minerals. Icarus. 180, 353-
564 358.
565 Lebofsky, L.A., Feierberg, M.A., Tokunaga, A.T., Larson, H.P. and Johnson, J.R., 1981. The 1.7-
566 to 4.2-micron spectrum of asteroid 1 Ceres: evidence for structural water in clay minerals.
567 Icarus. 48, 453–459.
568 Melchiorri, R., Encrenaz, T., Fouchet, T., Drossart, P., Lellouch, E., Gondet, B., Bibring, J.-P.,
569 Langevin, Y., Schmitt, B., Titov, D. and Ignatiev, N., 2007. Water vapor mapping on
570 Mars using OMEGA/Mars Express. Planet. Space Sci. 55. 333-342.
571 Michalski, J. R. and Niles, P. B., 2010. Deep crustal carbonate rocks exposed by meteoritic
572 impact on Mars. Nat. Geosci. 3, 751-755.

573 Milliken, R.E. and Rivkin, A.S., 2009. Brucite and carbonate assemblage from altered olivine-
574 rich materials on Ceres. Nat. Geosci. 2, 258-261.

575 Mittlefehldt, D.W., 1994. ALH84001, a cumulate othopyroxenite member of the Martian
576 meteorite clan. Meteoritics 29, 214–221.

577 Montes-H, G. and Geraud, Y. 2004. Sorption kinetic of water vapour of MX80 bentonite
578 submitted to different physical–chemical and mechanical conditions. Colloid Surface A.
579 235, 17-23.

580 Montes-H, G. and Rihs, S. 2006. A simplified method to estimate kinetic and thermodynamic
581 parameters on the solid–liquid separation of pollutants. J. Colloid Interf. Sci. 299, 49-55.

582 Montes-Hernandez, G., Fernandez-Martinez, A. and Renard, F. 2009. Novel Method to Estimate
583 the Linear Growth Rate of Submicrometric Calcite Produced in a Triphasic Gas-Liquid-
584 Solid System. Cryst. Growth Des. 9, 4567-4573.

585 Montes-Hernandez, G., Pommerol, A., Renard, F., Beck, P., Quirico, E. and Brissaud, O., 2010a.
586 In situ kinetic measurements of gas-solid carbonation of $Ca(OH)_2$ by using infrared
587 microscope coupled to a reaction cell. Chem. Eng. J. 161, 250-56.

588 Montes-Hernandez, G., Daval, D., Chiriac, R. and Renard, F., 2010b. Growth of Nanosied
589 Calcite through Gas-Solid Carbonation of Nanosized Portlandite under Anisobaric
590 Conditions. Cryst. Growth Des. 10, 4823-4830.

591 Montes-Hernandez, G., Chiriac, R., Toche, F. and Renard, F., 2012a. Gas–solid carbonation of
592 Ca(OH)2 and CaO particles under non-isothermal and isothermal conditions by using a

593 thermogravimetric analyzer: Implications for CO2 capture . Int. J. Greenh. Gas. Con. 11,
594 4172-180.

595 Montes-Hernandez, G., Daval, D., Findling, N., Chiriac, R. and Renard, F., 2012b. Linear growth
596 rate of nanosized calcite synthesized via gas–solid carbonation ofCa(OH)2 particles in a
597 static bed reactor. Chem. Eng. J. 180, 237-244

598 Morris, R.V., Ruff, S.W., Gellert, R., Ming, D.W., Arvidson, R. E.,Clark, B.C., Golden, D. C.,
599 Siebach, K., Klingelhöfer, G., Schröder, C., Fleischer, I., Yen, A.S. and Squyres, S.W.,
600 2010. Identification of Carbonate-Rich Outcrops on Mars by the Spirit Rover. Science
601 .329, 421-424.

602 Murchie, S.L., Mustard, J.F. Ehlmann, B.L., Milliken, R.E., Bishop, J.L., McKeown, N.K., Noe
603 Dobrea, E.Z., Seelos, F.P., Buczkowski, D.L., Wiseman, S.M., Arvidson, R.E., Wray, J.J.,
604 Swayze, G., Clark, R.N., Des Marais, D.J., McEwen, A.S. and Bibring, J.-P., 2009. A
605 synthesis of Martian aqueous mineralogy after 1 Mars year of observations from the Mars
606 Reconnaissance Orbiter. J.Geophys. Res.114, E00D06.

607 Mustard, J.F., Murchie, S.L., Pelkey, S.M., Ehlmann, B.L., Milliken, R.E., Grant, J.A., Birbing,
608 J.-P., Poulet, F., Bishop, J., Noe Dobrea, E., Seelos, F., Arvidson, R.E., Wiseman, S.,
609 Green, R., Humm, D., Malaret, E., McGovern, J.A., Seelos, K., Clancy, T., Clark, R., Des
610 Marais, D., Izenberg, N., Knudson, A., Langevin, Y., Martin, T., McGuire, P., Robinson,
611 M., Roush, T., Smith, M., Taylor, H., Titus, T. and Wolff, M., 2008. Hydrated silicate
612 minerals on Mars observed by the Mars Reconnaissance Orbiter CRISM instrument.
613 Nature. 454, 305-309

614 Ochs, D., Braun, B., Maus-Friedrichs, W. and Kempter, V. 1998a. CO2 chemisorption at Ca and

615 CaO surfaces: A study with MIES, UPS(HeI) and XPS. Surf. Sci .417,406–414.

616 Ochs, D., Brause, M., Braun, B., Maus-Friedrichs, W. and Kempter V.,1998b. CO2 chemisorp
617 tion at Mg and MgO surfaces: A study with MIES and UPS (He I). Surf .Sci., 397,101–
618 107.

619 Paquette, J. and Reeder, R.J., 1995. Relationship between surface structure, growth mechanism
620 and trace element incorporation in calcite. Geochem.Cosmochem. Acta. 59, 735-749.

621 Pommerol, A., Schmitt, B., Beck, P. and Brissaud, O., 2009. Water sorption on martian regolith
622 analogs: Thermodynamics and near-infrared reflectance spectroscopy. Icarus. 204, 114-
623 136.

624 Poulet, F., Bibring, J.-P., Langevin, Y., Mustard, J.F., Mangold, N., Vincendon, M., Gondet, B.,
625 Pinet, P., Bardintzeff, J.-M. And Platevoet, B., 2009. Quantitative compositional analysis
626 of martian mafic regions using the Mex/OMEGA reflectance data 1.Methodology,
627 uncertainties and examples of application. Icarus. 201, 69-83.

628 Rivkin, A.S., Volquardsen, E.L. and Clark, B.E., 2006. The surface composition of Ceres:
629 discovery of carbonates and iron-rich clays. Icarus. 185, 563–567

630 Rivkin, A.S., Li, J.Y., Milliken, R.E., Lim, L.F., Lovell, A.J., Schmidt, B.E., McFadden, L.A.
631 And Cohen, B.A., 2011. The surface composition of Ceres. Space Sci. Rev. 163, 95-116

632 Sala, M. , Delmonte, B., Frezzotti, M., Proposito, M., Scarchilli, C., Maggi, V., Artioli, G.,
633 Dapiaggi, M., Marino, F., Ricci, P.C. and De Giudici, G., 2008. Evidence of calcium
634 carbonates in coastal (Talos Dome and Ross Sea area) East Antarctica snow and firn:
635 Environmental and climatic implications. Earth Planet. Sci. Lett. 271, 43-52.

636 Santos, A., Ajbary, M., Morales-Flórez, V., Kherbeche, A., Pi˜nero, M. and Esquivias, L., 2009.
637 Larnite powders and larnite/silica aerogel composites as effective agents for CO2
638 sequestration by carbonation. J. Hazard. Mater. 168, 1397–1403.

639 Schorghofer, N. and Aharonson, O., 2005. Stability and exchange of subsurface ice on Mars. J.
640 Geophys. Res. 110, E05003.

641 Shaheen, R., Abramian, A., Horn, J., Dominguez, G., Sullivan, R. and Thiemens, M. H., 2010.
642 Detection of oxygen isotopic anomaly in terrestrial atmospheric carbonates and its
643 implications to Mars. Proceedings of the National Academy of Sciences of the United
644 States of America 107, 20213-20218.

645 Sigg, L., Xue, H., Kistker, D. and Schönenberger, R., 2000. Size fractionation (dissolved,
646 colloidal and particulate) of trace metals in the Thur River, Switzerland. Aquat. Geochem.
647 6, 413-434

648 Smith, M.D., 2002. The annual cycle of water vapor on Mars as observed by the Thermal
649 Emission Spectrometer. J. Geophys. Res. 107, E11,5115.

650 Smith, M.D., 2004. Interannual variability in TES atmospheric observations of Mars during
651 1999-2003. Icarus. 167, 148-165.

652 Smith, M.D., Wolff, M.J., Clancy, R.T. and Murchie, S.L., 2009. Compact Reconnaissance
653 Imaging Spectrometer observations of water vapor and carbon monoxide. J. Geophys.
654 Res. 114, E00D03.

655 Smith, P.H., Tamppari, L.K., Arvidson, R.E., Bass, D., Blaney, D., Boynton, W.V., Carswell, A.,
656 Catling, D.C., Clark, B.C., Duck, T., DeJong, E., Fisher, D., Goetz, W., Gunnlaugsson,
657 H.P., Hecht, M.H., Hipkin, V., Hoffman, J., Hviid, S.F., Keller, H.U., Kounaves, S.P.,

Lange, C.F., Lemmon, M.T., Madsen, M.B., Markiewicz, W.J., Marshall, J., McKay, C.P., Mellon, M.T., Ming, D.W., Morris, R.V., Pike, W.T., Renno, N., Staufer, U., Stoker, C., Taylor, P., Whiteway, J.A. and Zent, A.P., 2009. H_2O at the Phoenix Landing Site. Science .325, 58-61.

Stumm, W. and Morgan, J.J., 1995. , Aquatic Chemistry – Chemical Equilibria and Rates in Natural Waters, John Wiley & Sons Inc., Third Edition, New York.

Thomas, P.C., Parker, J.Wm., McFadden, L.A., Russel, C.T., Stern, S.A., Sykes, M.V. and Young, E.F., 2005. Differentiation of the asteroid Ceres as revealed by its shape. Nature. 437, 224-226.

Treiman, A. H., Amundsen, H. E. F., Blake, D. F. and Bunch, T., 2002. Hydrothermal origin for carbonate globules in Martian meteorite ALH84001: a terrestrial analogue from Spitsbergen (Norway). Earth Planet. Sci. Lett. 204, 323-332.

Vernazza, P., Mothé-Diniz, T., Barucci, M.A., Birlan, M., Carvano, J.M., Strazzulla, G., Fulchignoni, M. and Migliorini, A., 2005. Analysis of near-IR spectra of 1 Ceres and 4 Vesta, targets of the Dawn mission. Astron. Astrophys. 436, 1113–1121.

Xiong, Y. and Snider Lord, A., 2008. Experimental investigations of the reaction path in the MgO-CO_2-H_2O system in solutions with various ionic strengths, and their applications to nuclear waste isolation. App. Geochem. 23, 1634–1659.

Yamamoto, S., Bluhm, H., Andersson, K., Ketteler, G., Ogasawara, H., Salmeron, M. and Nilsson, A., 2008. In situ X-ray photoelectron spectroscopy studies of water on metals and oxides at ambient conditions. J. Phys. Condens. Matt., 20, 184025-184014.

Zolensky, M.E., Nakamura, K., Gounelle, M., Mikouchi, T., Kasama, T., Tachikawa, O. and Tonui, E., 2002. Mineralogy of Tagish Lake : An ungrouped type 2 carbononaceous chondrite. Meteorit. Planet. Sci. 37, 737-761.

703 Table 1. Summary of the experiments with their experimental conditions and the corresponding
704 kinetic parameters determined for gas-solid carbonation.

Exp.	Starting material	Gas pressure	temperature	$A^{CO3}_{,max1}$ (a.u.)	$A^{CO3}_{,max2}$ (a,u,)	$t_{1/2_1}$ (minutes)	$t_{1/2_2}$ (minutes)	Ea (kJ/mol)
1	portlandite	2 bar CO_2	-10°C	1.8	4.6	19.6	599.6	
2	portlandite	2 bar CO_2	0°C	6.4	0.8	8.9	8.9	43
3	portlandite	2 bar CO_2	10°C	5.3	11.4	61.8	61.8	
4	portlandite	2 bar CO_2	25°C	29.3	54.8	2.5	126.6	
5	portlandite	1 bar CO_2 + air	-10°C	2.5	5	3.7	33622	
6	portlandite	1 bar CO_2 + air	0°C	5.4	10.2	6.3	28.5	75
7	portlandite	1 bar CO_2 + air	10°C	15.8	3.1	3.5	180.1	
8	portlandite	1 bar CO_2 + air	30°C	26	21.2	3.5	5.8	
9	portlandite	100 mbar CO_2	25°C	19.8	10.9	0.8	419.1	
10	brucite	1 bar CO_2 + air	25°C	9.5	4.8	3	184.1	
11	Amorphous Ca silicate hydrate	1 bar CO_2 + air	25°C	8.9	68	<0.5	13.6	

Ea was calculated with Arrhenius equation. For experiments with 2 bar CO_2 ,we exclude the point of 10°C due to his incoherence with Arrhenius equation.

705

706

707

708

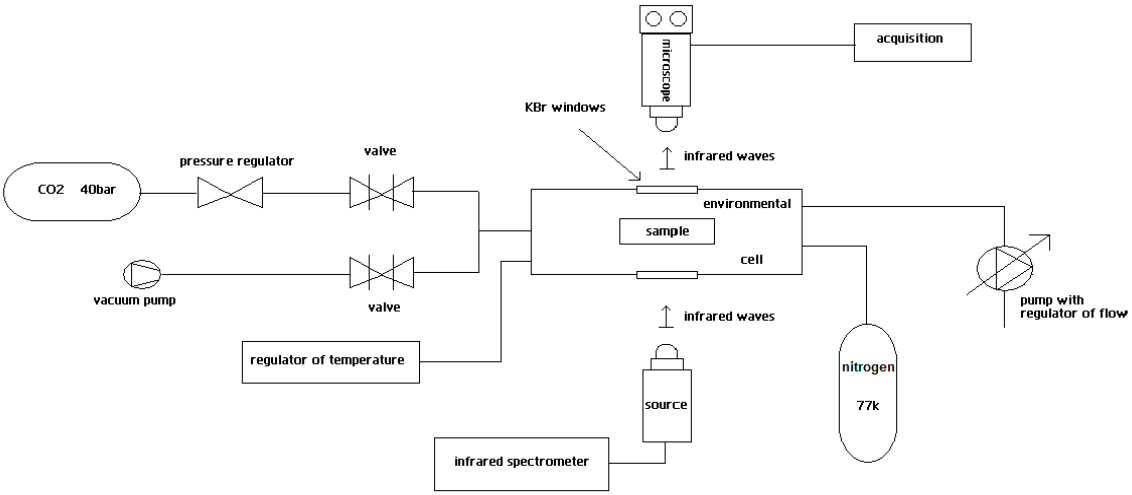

709

710

711

712

713

714 **Figure 1 .** Schematic representation of the IR-CryoCell experimental setup, showing the main
715 parts such as temperature regulator, environmental cell, infrared microscope, valves, vacuum
716 pump, CO_2 cylinder, liquid N_2 reservoir.

717

718

719

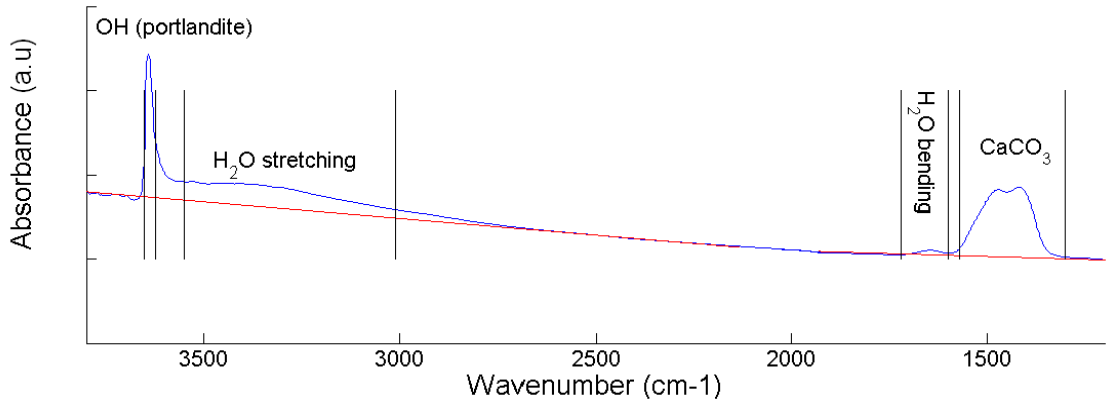

720

721

722 **Figure 2 .** Schematic representation for the calculation of the integrated band intensities of each
723 functional group (-OH, H_2O, MCO_3), showing the continuum (in red) on an IR spectrum of
724 portlandite.

725

726

727

728

729

730

731

732

733

734

735

736

737

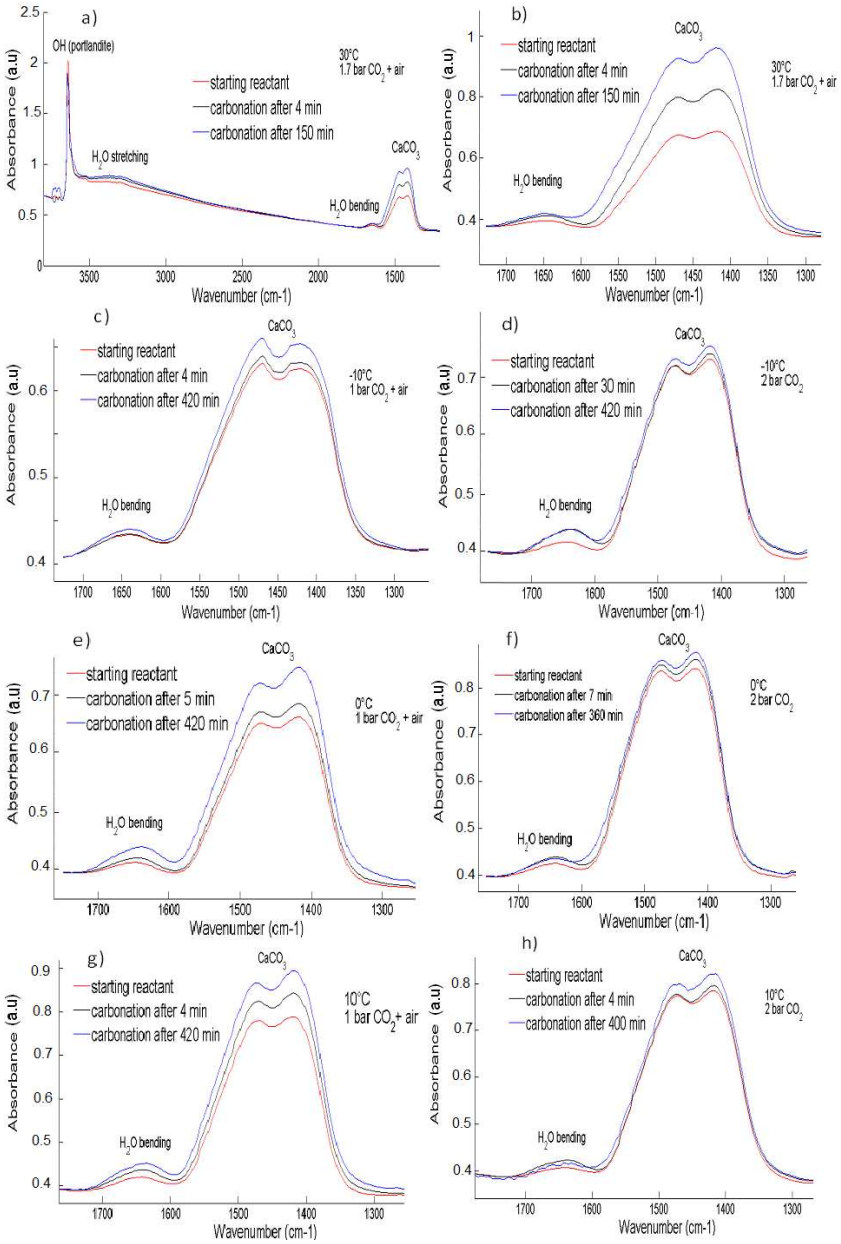

738

739 **Figure 3.** Evolution with time of the IR spectrum of calcium carbonate during carbonation at
740 different temperatures and CO_2 pressures. a) Full IR spectrum of portlandite at 30°C with 1.7 bar
741 of CO_2 in presence of air; (b) Carbonate band at 30°C under 1,7 bar of CO_2 with air; (c) at -10°C
742 under 1bar of CO_2 with air ; (d) at -10°C under 2 bars of CO_2; (e) at 0°C under 1bar of CO_2 with
743 air ; (f) at 0°C under 2bars of CO_2; (g) at 10°C under 1bar of CO_2 with air; (h) at 10°C under
744 2bars of CO_2.

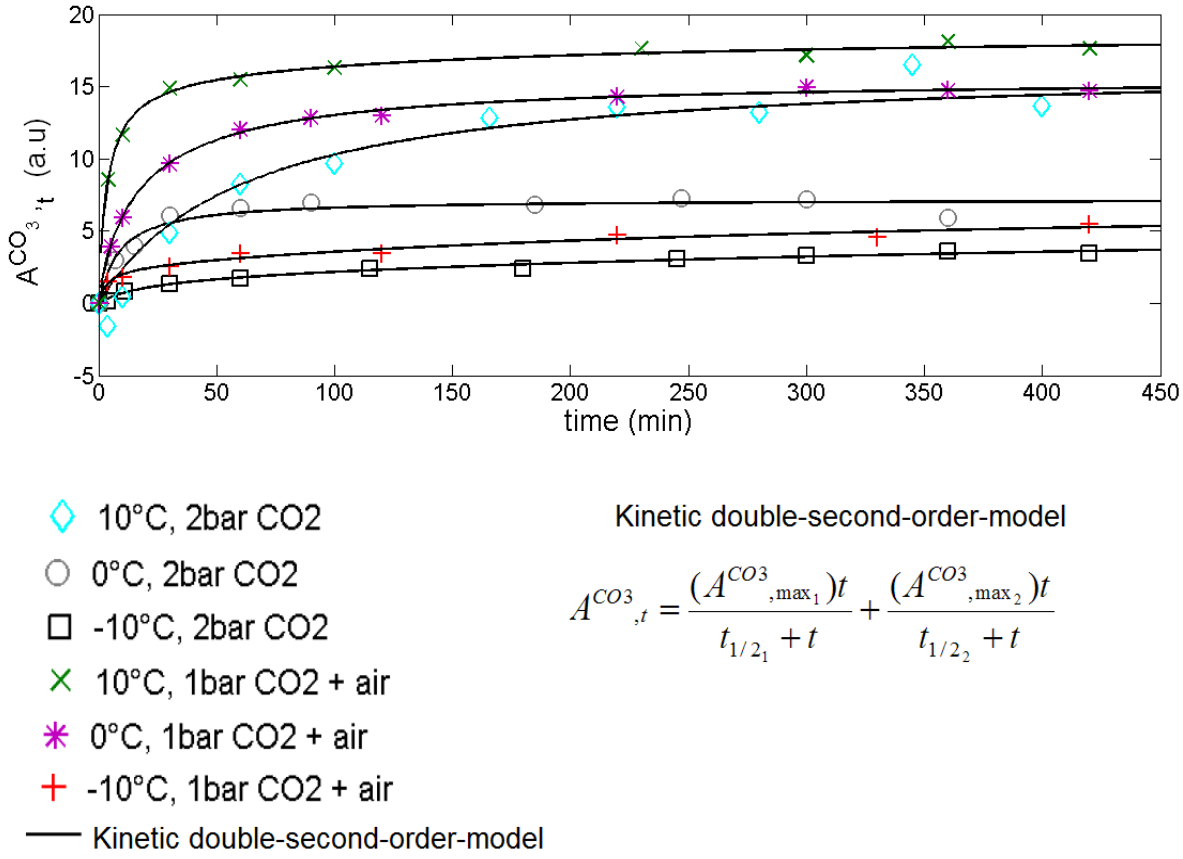

745

746

747

748 **Figure 4.** Fits of the experimental kinetic data (carbonate band intensity) for gas-solid
749 carbonation of Ca hydroxide (portlandite) in various experimental conditions by using a kinetic
750 double-pseudo-second-order model and applying the non-linear least squares method.

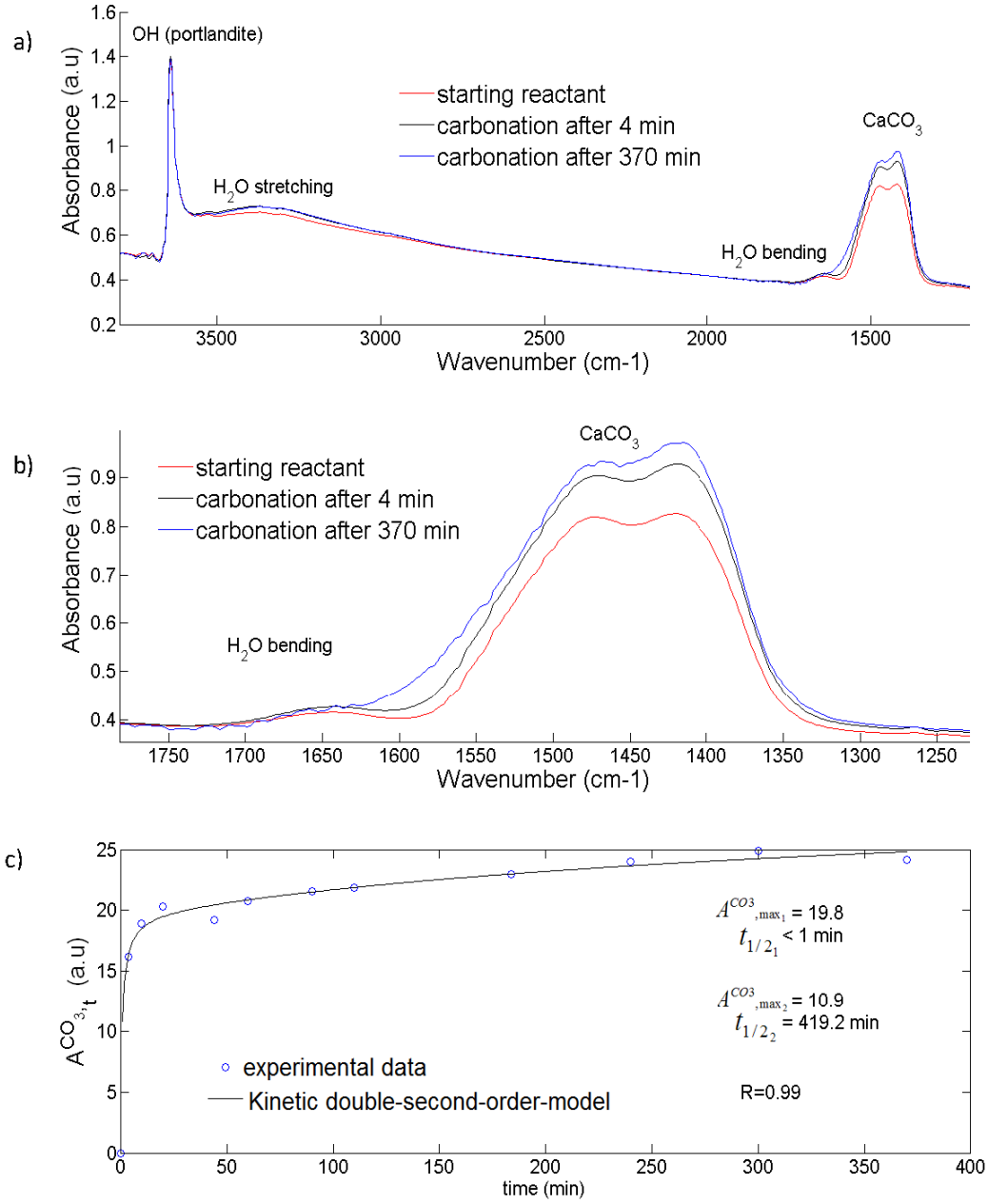

751 **Figure 5.** Evolution with time of the IR spectrum of Ca hydroxide (portlandite) during
752 carbonation at 25°C under 100mbar of CO_2: a) Full spectrum. b) Band of the carbonate group. c)
753 Fit of the experimental kinetic data (carbonate band intensity) for gas-solid carbonation by using
754 a kinetic double-pseudo-second-order model and applying the non-linear least squares method.

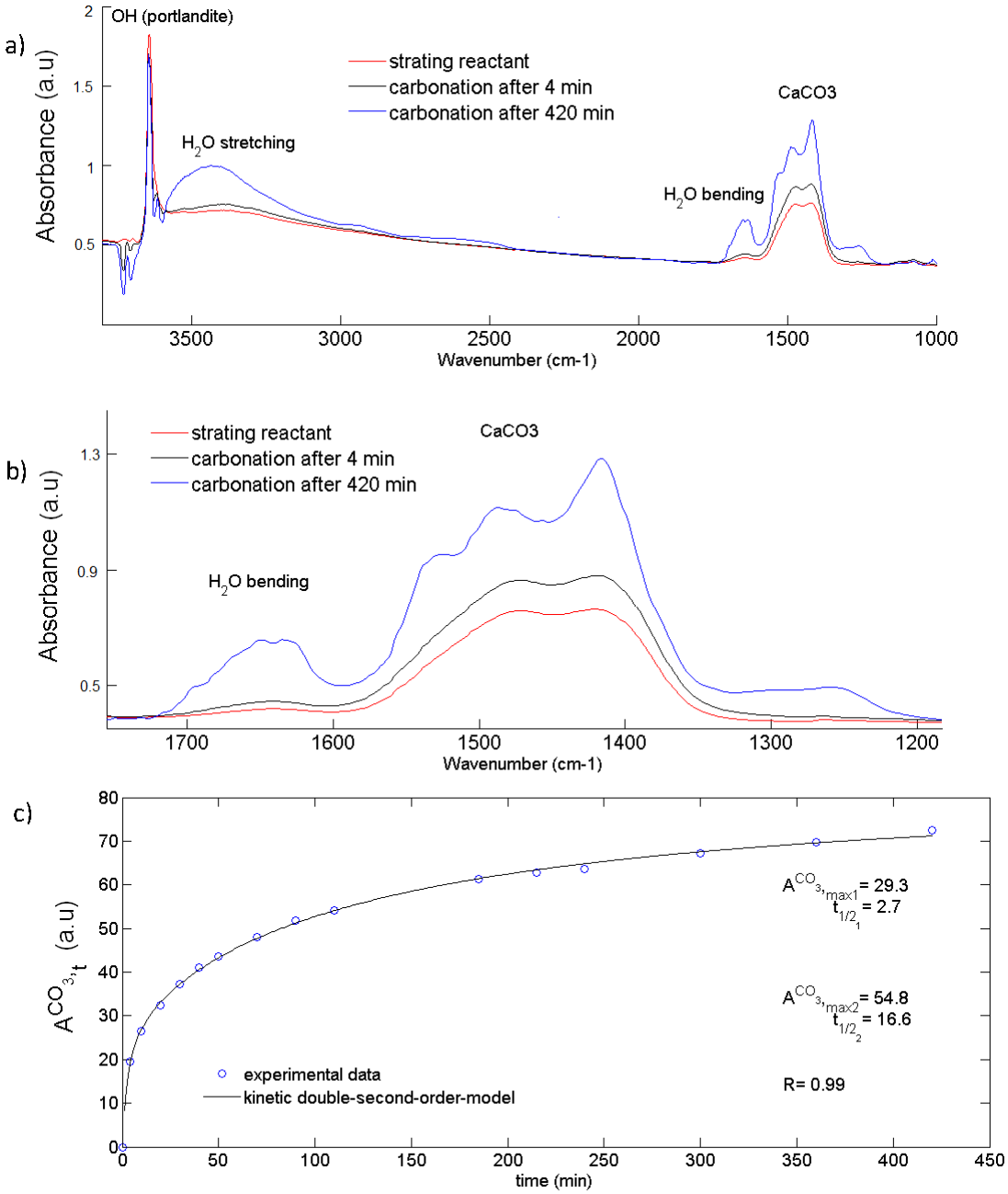

755

756 **Figure 6.** Evolution with time of the IR spectrum of Ca hydroxide (portlandite) during
757 carbonation at 25°C under 2 bar of CO_2: a) Full spectrum. b) Band of the carbonate group. c) Fit
758 of the experimental kinetic data (carbonate band intensity) for gas-solid carbonation by using a
759 kinetic double-pseudo-second-order model and applying the non-linear least squares method.

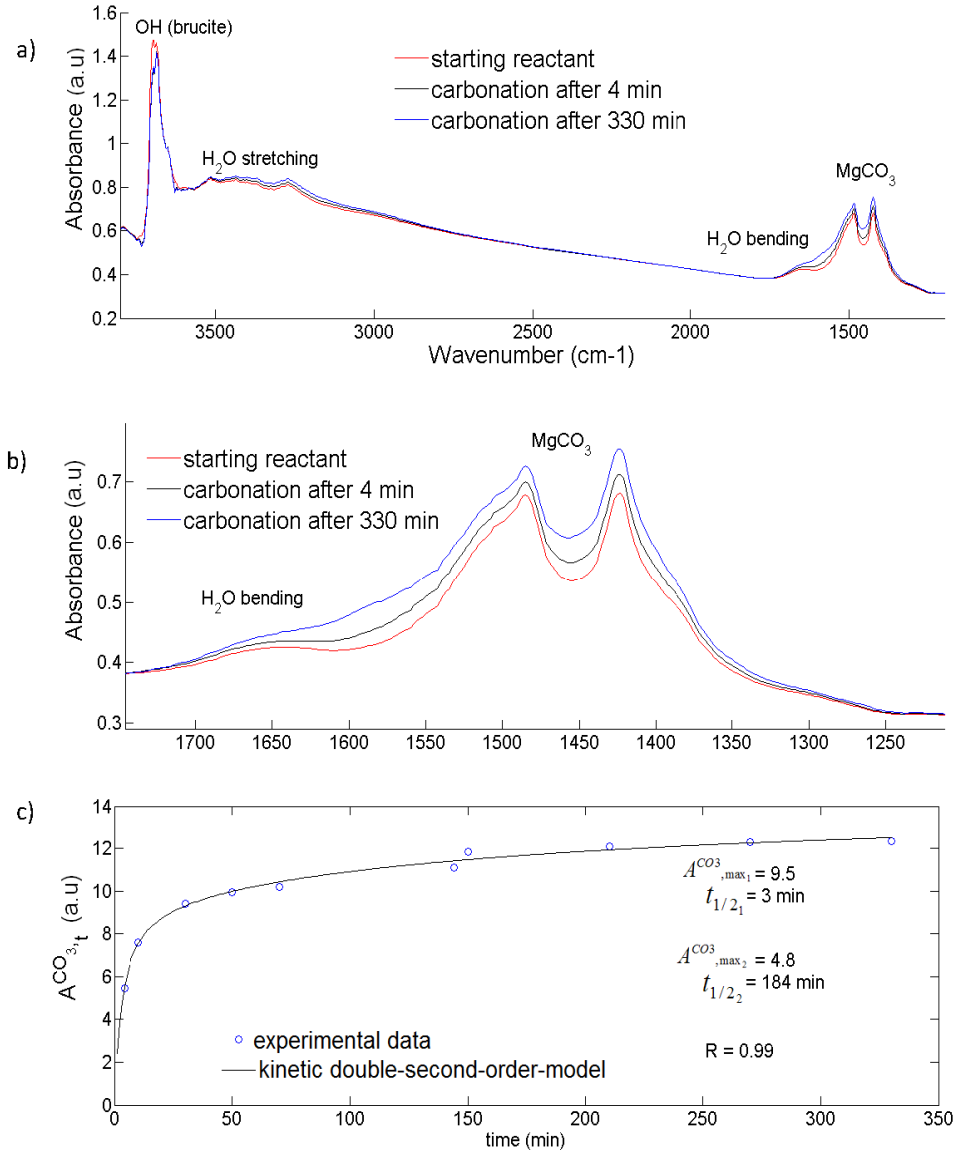

760

761 **Figure 7.** Evolution with time of the IR spectrum of the Mg hydroxide (brucite) during
762 carbonation at 25°C under 1bar of CO_2 with air: a) Full spectrum. b) Band of the carbonate group
763 c) Fit of the experimental kinetic data (carbonate band intensity) for gas-solid carbonation by
764 using a kinetic double-pseudo-second-order model and applying the non-linear least squares
765 method.

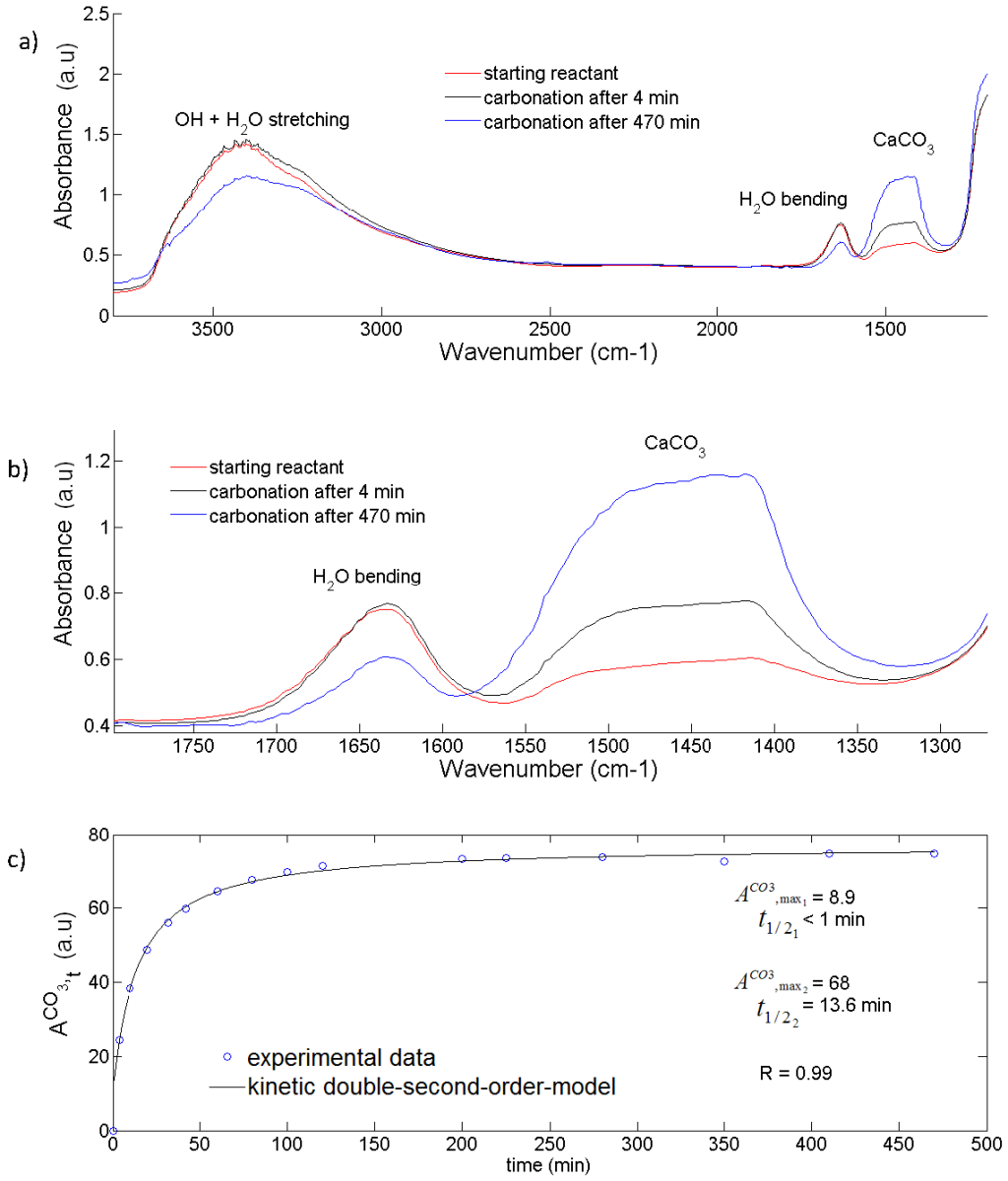

766

767 **Figure 8.** Evolution with time of the IR spectrum of amorphous Ca silicate hydrate during
768 carbonation at 25°C under 1bar of CO_2 with air: a) Full spectrum. b) Band of carbonate group. c)
769 Fit of the experimental kinetic data (carbonate band intensity) for gas-solid carbonation by using
770 a kinetic double-pseudo-second-order model and applying the non-linear least squares method.

771

772

773

774

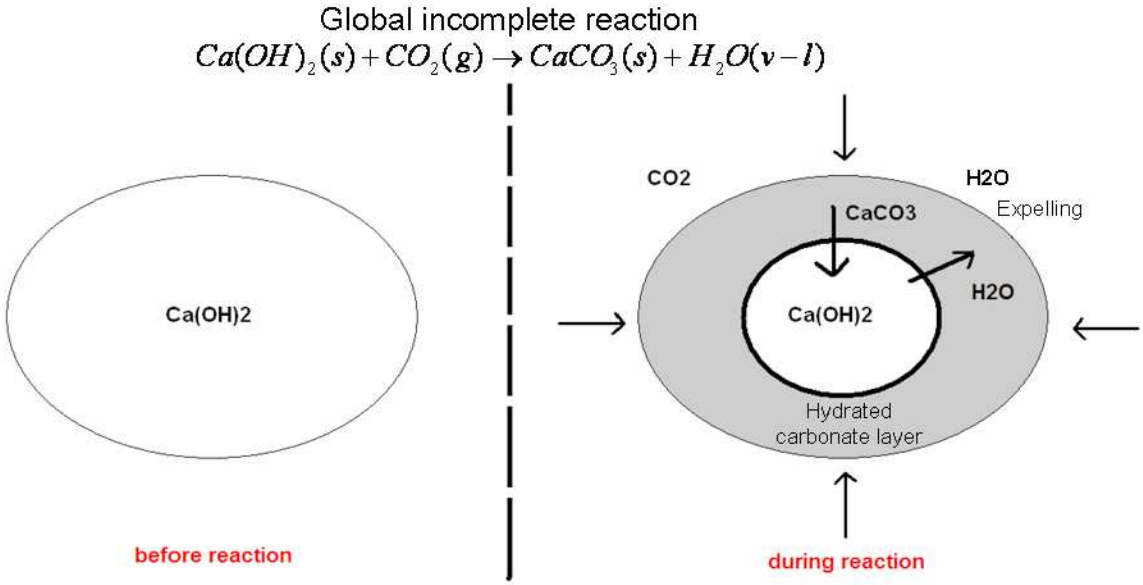

775

776 **Figure 9.** Schematic representation of the gas-solid carbonation of Ca hydroxide, showing the
777 growth of a hydrated calcium carbonate layer and the expelling of molecular water.

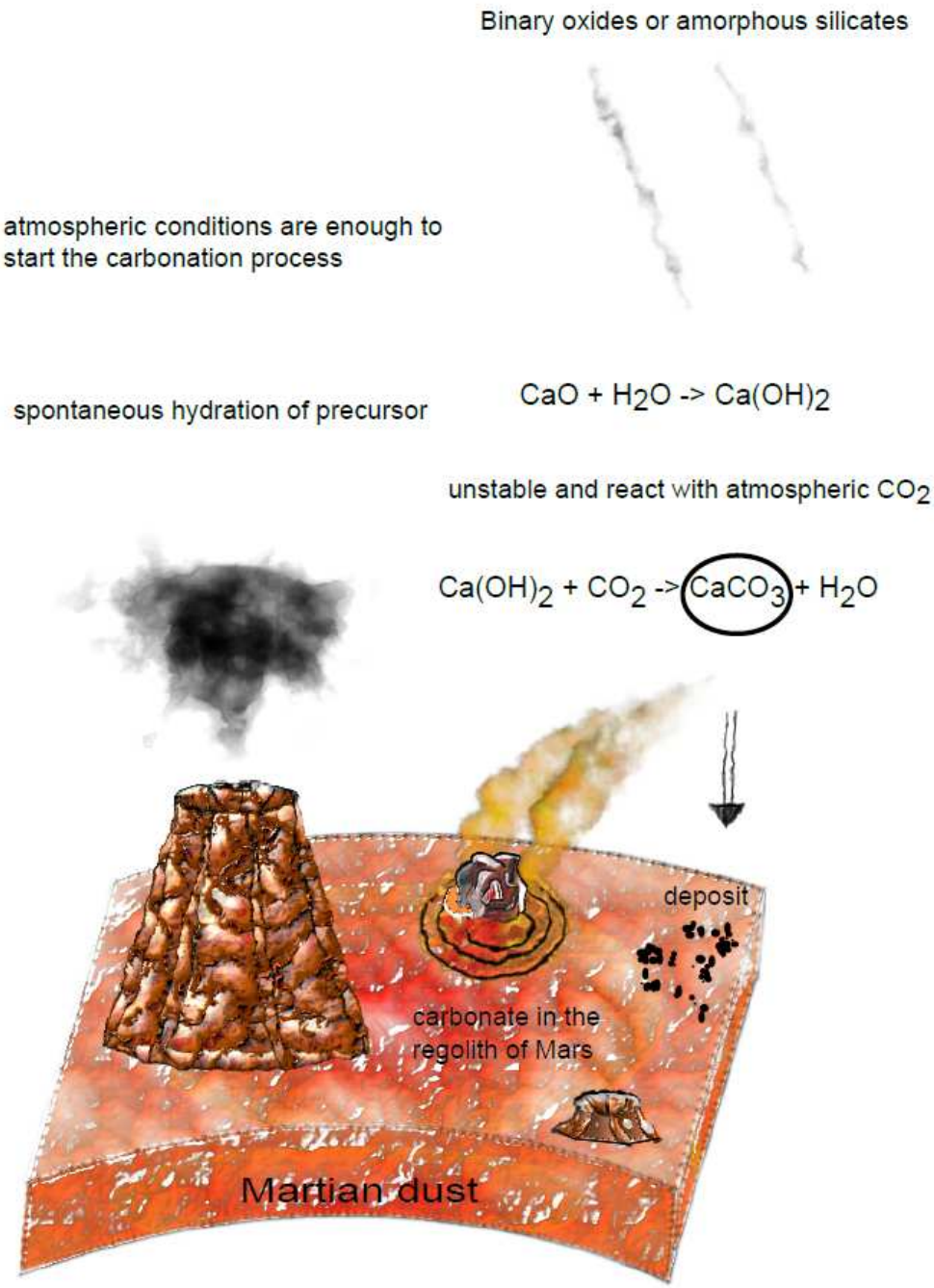

778

779

780

781 **Figure 10.** A schematic representation of a possible current formation mechanism at dust-CO2
782 interfaces of the calcium carbonate found at the Martian surface.